Compressive Sensing Imaging through Atmospheric Turbulence

Gabriela Paunescu, Daniel Wegner, Peter Lutzmann, Endre Repasi
Fraunhofer Institute of Optronics, System Technologies and Image Exploitation (IOSB),
Department Optronics, Gutleuthausstrasse 1, 76275 Ettlingen
GERMANY

gabriela.paunescu@iosb.fraunhofer.de

ABSTRACT

Compressive sensing (CS) can often provide a solution for the lack of suitable camera technologies in certain spectral wavelength ranges, especially for active imaging systems. Atmospheric turbulence degrades FPA based electro-optic imaging systems due to intensity fluctuation, distortion, and blur, notably for long-range applications. CS imaging techniques are assumed to be less sensitive to atmospheric turbulence than conventional systems. However, to date no comparative investigation on the turbulence influence on both types of systems is available to prove this. In this paper, we present the first results of laboratory measurements how turbulence affects the image quality using CS techniques in the SWIR spectral range in comparison to a conventional InGaAs-FPA based camera.

1.0 INTRODUCTION

Compressive sensing (CS) is a computational imaging method increasingly investigated in recent years[1,2]. In a CS image acquisition, a high-resolution image is recovered from a series of specifically designed measurements. Each measurement consists of low resolution acquisitions after image coding by defined patterns. The reconstruction of the high resolution image requires a number of measurements significantly smaller than the number of whole-image pixels. The main advantage of the technique is the possibility to replace expensive matrix detectors by small and cheap detectors containing only one or a few elements. This is primarily relevant for spectral ranges where large format focal plane array (FPA) sensors are not available, e. g. THz and X-ray imaging. Even for spectral ranges with well-established sensing methods such as visible or SWIR, CS technology may be designed to efficiently extract specific information from a scene.

Numerous optical applications require imaging through atmospheric turbulence. This degrades FPA based electro-optic imaging systems due to intensity fluctuation, distortion, and blur, notably for long-range applications. The sensitivity of CS imaging techniques to atmospheric turbulence has not been rigorously investigated so far. To date, no comparative study on the turbulence influence on both types of systems is available.

This paper presents laboratory measurements how turbulence affects the image quality using CS techniques in the SWIR spectral range in comparison to a conventional InGaAs-FPA based camera. Operational parameters (integration time, resolution etc.) were as close as possible for both systems. Strong turbulence conditions created by using a heating plate placed under the propagation paths formed the basis for the experiment. The turbulence affected the acquisition of a test target. Analyses of signal fluctuation and position of this test target allowed quantifying the influence of the turbulence. The resulting data allowed comparisons with and without turbulence and in-between the two different system concepts.

2.0 COMPRESSIVE SENSING EXPERIMENTS

2.1 Compressive Sensing Setup

Fig. 1 shows the experimental setup[3]. The illuminated scene is imaged onto the digital mirror device (DMD) by a lens with 100 mm diameter and 60 mm focal length. The target is placed at a distance of 2.5 m from the imaging lens. The DMD used to generate binary patterns is a V7001 model from Texas Instruments and contains 1024 x 768 micromirrors with a pitch of 13.7 µm. Each micromirror may be set at two angle states (+/- 12°), generating binary pixel values (1/0) for the coding pattern. The light modulated by the applied pattern will be reflected at 12°, while the complementary pattern will modulate the reflection at -12°. Each reflection is collected using a parabolic mirror and a condenser lens and recorded by a single element (bucket) detector. Typically, the image is reconstructed using the signal from one detector. Either the signal modulated by the applied patterns, or the signal modulated by the complementary patterns, may be used for the image reconstruction. However, the simultaneous recording of both signals provides advantages. The sum of the signals may function as a correction factor for the illumination light intensity variations[4]. An improvement of reconstructed image quality using the difference of the two acquired signals was demonstrated[5,6]. This also attenuates the influence of the background light if the complementary signals are simultaneously acquired[7]. Furthermore, the setup allows simultaneous image acquisition in two different spectral ranges if suitable detectors are inserted[8].

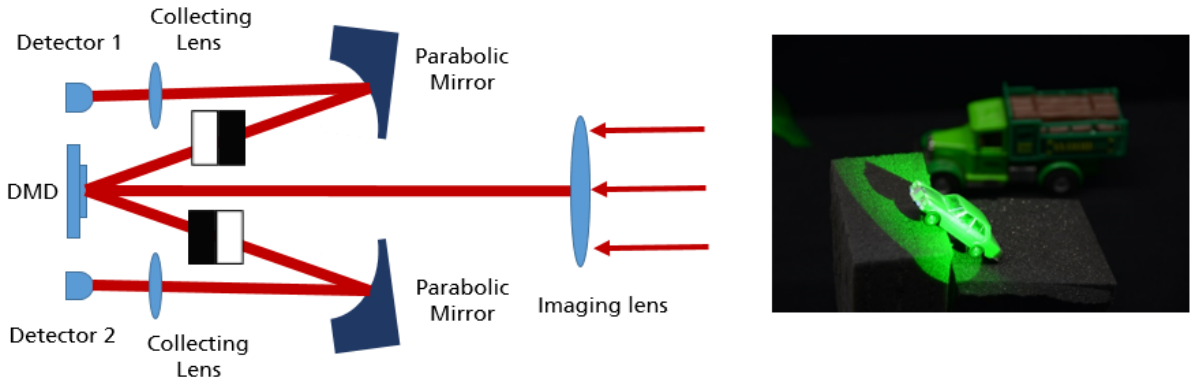

Figure 1: Experimental setup used for compressive sensing (CS) measurements, DMD: digital micromirror device.

The setup was applied in both visual (VIS) and short wave infrared (SWIR) spectral ranges using different illumination sources and appropriate bucket detectors. Table 1 summarizes the investigated experimental configurations. First experiments have been performed under continuous illumination, using both non-coherent (halogen lamp) and coherent sources (CW lasers), in VIS as well as in SWIR. When the object is illuminated with a halogen lamp, both VIS and SWIR spectral ranges could be covered simultaneously because of the broad overall spectrum. The listed spectral ranges (Table 1) refer to the overlap in spectral range of the illumination sources and detector sensitivities.

Table 1. Illumination sources and bucket detectors.

Light source	Detector	Overlap spectral range
Halogen lamp	Si photodiode	VIS: 350 – 1100 nm
Halogen lamp	InGaAs photodiode	SWIR: 800 – 1700 nm
CW laser	Si photodiode	VIS: 532 nm
CW laser	InGaAs photodiode	SWIR: 1550 nm
Pulse laser	InGaAs photodiode	SWIR: 1550 nm

The pulsed laser used for the measurements is a fiber laser that delivers 10 ns pulses with up to 120 µJ energy at a center wavelength of 1550 nm. The laser may be externally triggered from single pulse to a maximal pulse repetition rate of 20 kHz. The main laser parameters are listed in Table 2. The trigger output signal of the DMD was used to control the laser emission and to synchronize the data acquisition with the laser pulse. A 1 Gsample/s digitizer was used to record the signal from detectors. The entire measurement system was controlled via LabVIEW software.

Table 2. Parameters of laser used for scene illumination.

Pulse laser parameters	
Center wavelength	*1550 nm*
Spectral width (FWHM)	*20 nm*
Pulse width (FWHM)	*10 ns*
Pulse repetition frequency	*single shot to 20 kHz*
Maximum pulse energy	*120 µJ*
Beam propagation factor M^2	*< 1.5*
Beam polarization	*random*

2.2 Image reconstruction

The binary patterns used to modulate the object back reflected light have been generated using the Hadamard matrix of N x N dimension, where N is the number of pixels in the reconstructed image. For a full-resolution measurement, each row of the matrix is resized to create a pattern of $\sqrt{N} \times \sqrt{N}$ pixels. For CS image reconstruction a smaller pattern number (M<N) is required. Selection of the patterns has a strong influence on the image quality and on the minimum number of measurements necessary to fulfil some defined requirements[9]. The M patterns have been selected using four different strategies:

Method A: *Sequency ordered patterns*

The first M patterns in the sequency ordered Hadamard matrix have been selected. The rows of the sequency ordered matrix are arranged in increasing order of sign-changes or zero-crossings[10].

Method B: *Scene adapted pattern selection*

The second method used for patterns selection is a kind of “evolutionary compressive sensing”, in which the patterns are ordered after a full-resolution measurement has been performed[8]. The relevance of a pattern for the imaged scene is evaluated according to the following considerations. The Hadamard matrix based binary

patterns have equally distributed +/-1 pixel values excepting the first pattern in which all pixels are "1". A normed measured signal of a uniform target is a constant signal of 0 excepting the first point of 1; therefore it is assumed that the scene features are contained in measurements far away from the mean value. The patterns are ordered according to the absolute values of the difference between signal and mean value. The method will be further referred as "scene adapted pattern selection".

Method C: *Image collection relevant patterns*

The method B has the disadvantage that a full resolution measurement should be performed first in order to subsequently select the appropriate patterns. Therefore the next step was to analyse the relevance of the patterns for an image data base. The index of a pattern was evaluated according to the previous method for 64 images of arbitrary scenes and objects. Finally the patterns are ordered by their averaged index and the first M patterns are selected.

Method D: *Numbers of blocks ordered patterns*

Another investigated method was to order the patterns by the number of blocks they contain. A block is defined as a rectangle of pixels with the same value. The method is equivalent to assorting after increasing order of zero-crossing in the resized rows (2D patterns). A higher number of blocks in the patterns is associated with a higher spatial resolution.

The pixel values x in the image have been reconstructed by minimizing the function

$$F(x) = \|\Phi x - b\|_2^2 \qquad (1)$$

Φ is a matrix with M x N dimension containing the M modulation patterns each with N pixels and b is a vector of size M containing the corresponding measurements. The minimizer uses a conjugate gradient method based on the Fletcher-Reeves update formula[11] in combination with Golden Section line search[12].

The resolution of the reconstructed image is defined by the resolution of the binary patterns applied on the DMD. For the measurements under pulse laser illumination, binary patterns with 256 x 256 pixels have been used to modulate the collected light. Each pixel combines 3 x 3 micromirrors, so the active DMD area contains 768 x 768 micromirrors and has a size of 10.5 x 10.5 mm^2. The imaged scene was placed at 2.5 m from the collecting lens and illuminated with one pulse with 4 μJ pulse energy per applied pattern. Fig. 2 left shows an image of the test objects taken with a still camera; the camera viewing angle is slightly different from the CS system viewing angle. A full-resolution image reconstruction is shown in Fig. 2 right.

Figure 2: Image of the test objects taken with a DSLR camera (left) and a full-resolution reconstruction using the CS setup (right).

Undersampled reconstructions have been performed for M/N ("compression ratio") values of 50% and lower. Fig. 3 displays a set of reconstructed images with different compression ratios. The modulation patterns have been selected using the method B.

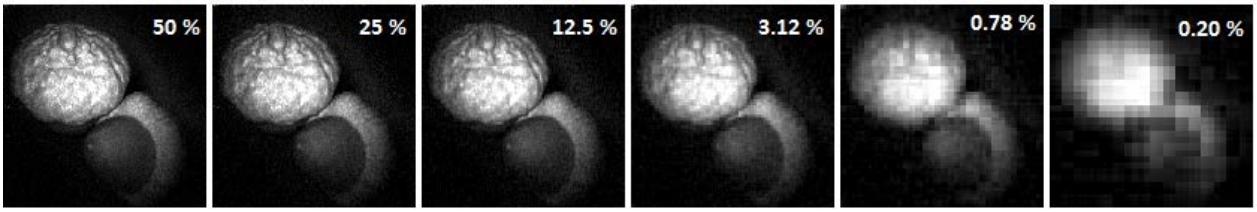

Figure 3: Reconstructed images with different compression ratios using the scene adapted pattern selection.

For a more rigorous and quantitative evaluation of the reconstructed images, two image quality metrics have been calculated: structural similarity (SSIM) index[13] and mean-squared error (MSE). Each metric relies on comparison with a reference image. The full-resolution reconstructed image (Fig. 2 right) was used as pristine image for the computations. Fig. 4 shows a comparison of the four methods used for pattern selection. The SSIM and MSE plots versus compression ratio evidence the superiority of the scene adapted pattern selection (method B) over the other methods. However, the methods C and D come close to B and may be successfully implemented when the aquisition time is a critical parameter.

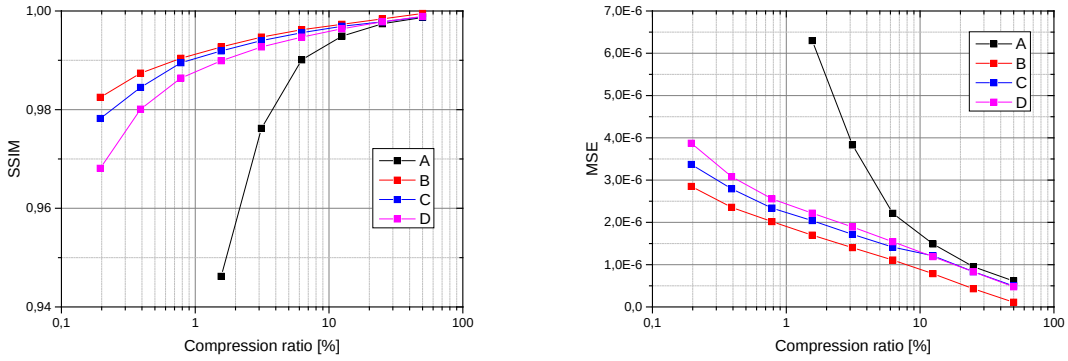

Figure 4: Structural similarity index SSIM (left) and mean-squared error MSE (right) as functions of compression ratio M/N for the four methods used to select the patterns. A: sequency ordered patterns; B: image adapted pattern selection; C: image collection relevant patterns; D: number of blocks ordered patterns.

3.0 COMPRESSIVE SENSING IMAGING TROUGH TURBULENCE

3.1 Experimental configuration

Effects of air turbulence on the image reconstruction via compressive sensing technique have been experimentally investigated in laboratory conditions. Strong local turbulence has been generated using a heating plate placed under the propagation path. The compressive sensing system described in Section 2.1 was used for image acquisitions of a target, both under normal and strong air turbulence conditions. Simultaneously, a FPA-camera recorded images of the same target. Fig. 5 shows the experimental configuration. The target was placed at about 2.5 m from the imaging lenses and illuminated by a halogen lamp. The 50 cm long heating plate was arranged along the propagation axis about 40 cm from the target, so that the illumination light to not be perturbed by the generated turbulence. The camera viewing angle is slightly different from the CS system viewing angle. The parameters of both imaging systems (Table 3) have been chosen to assure similar values of the instantaneous field of view (IFOV).

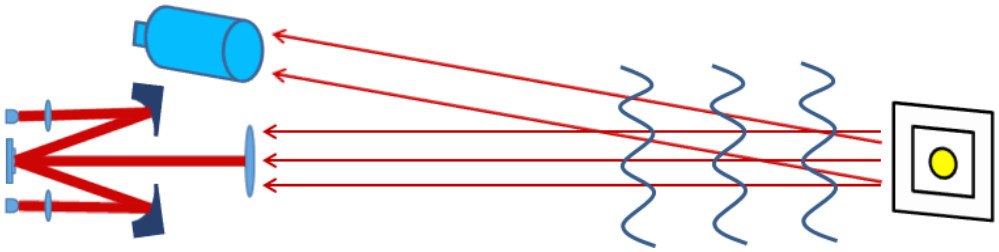

Figure 5: Experimental setup used for compressive sensing (CS) measurements. DMD: digital micromirror device.

Table 3. Parameters of compared imaging systems.

	Compressive Sensing	**SWIR Camera**
Detector	InGaAs single element (2x)	InGaAs - FPA
Resolution	256 x 256	640 x 512 (256 x 256 used)
Pixel Size	41.1 µm (3 x 3 micromirrors pro pixel)	25 µm
Optics	600 mm / f/6	400 mm / f/4
IFOV	68.5 µrad	62.5 µrad

3.2 Data acquisition

To evaluate the turbulence induced effects, a target containing a disc surrounded by a geometrical pattern was chosen. Fig. 6 shows the electronically generated pattern (a), its image recorded by the FPA-camera (b) and a full-resolution image reconstruction using the CS system (c). Sequences of images have been recorded using the CS system and the FPA-based camera, both under normal and turbulent conditions. Using the CS technique, images with a 256 x 256 pixel resolution have been reconstructed from 16000 measurements corresponding to a compression ratio of about 25%. The applied patterns were based on the Hadamard matrix and have been selected using different methods, as explained in Section 2.2. The DMD was driven with 4 kHz frame rate corresponding to a measurement time of about 4 s. The system allowed the acquisition of an image every 30 s.

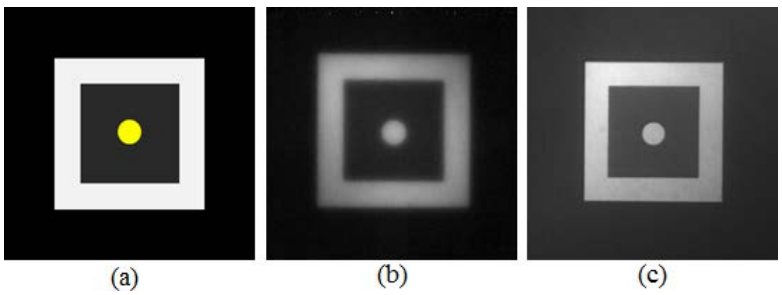

Figure 6: (a) Test Target. (b) Full resolution reconstruction using the CS setup. (c) FPA-camera image.

3.3 CS Measurements through turbulence

The influence of laboratory-generated turbulence on the target imaging could be live observed in the SWIR-camera recordings. The strongest effect occurring was the so-called image dancing. In addition, image blur and distortion could be intermittently observed. By performing CS measurements under the same conditions, the signals acquired by both single-pixel detectors experience strong perturbation. If only one of the signals is used for image reconstruction, this perturbation is converted in high image noise, as displayed in Fig. 7. However, using the difference between the two simultaneously acquired signals, the image noise could be almost totally eliminated. This indicates a time varying, spatially uniform perturbation which is most likely caused by the background SWIR radiation generated by the heating plate. Therefore, for further analysis and comparison with the FPA camera, only double channel measurements will be considered.

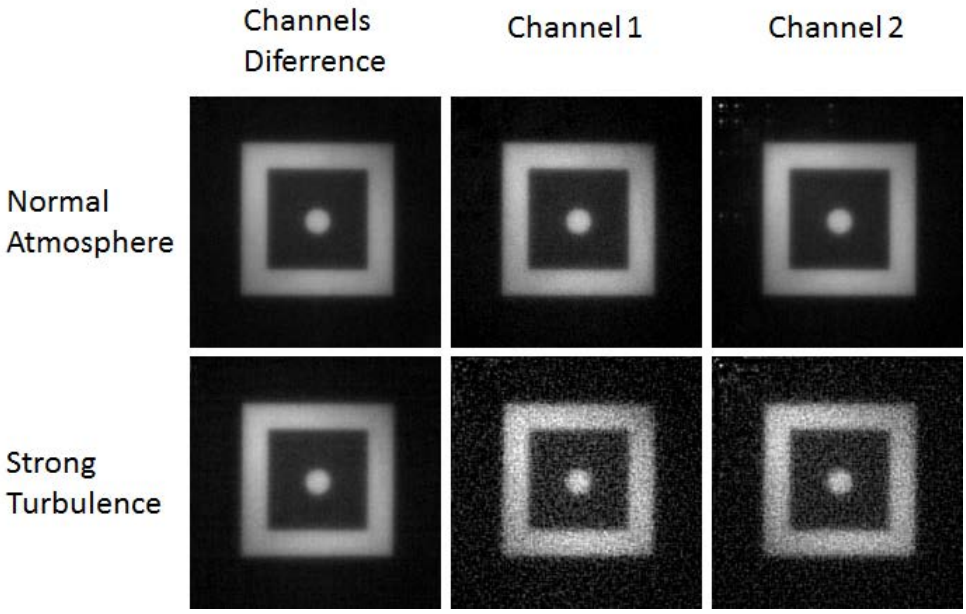

Figure 7: Image reconstructions under normal and strong turbulence conditions using single and double channel signals. Resolution: 256 x 256 pixels. Compression ratio ~ 25%.

3.4 Data fitting

In order to compare the SWIR camera and the CS system under the influence of turbulence effects, we measure projections of the input scenery containing a single circle with a surrounding square frame (Fig. 6a). Fixed regions of interest containing only the circle are cropped from the captured FPA-images and the CS reconstruction images.

Then pixel data within these regions of interests is fitted by a model function:

$$I_{circle}(x,y) = c_{background} + c_{circle} \cdot sigmoid\left(s, \sqrt{(x-x_0)^2 + (y-y_0)^2}, r_0\right), \qquad (2)$$

where x and y are integer pixel coordinates, $c_{background}$ is a constant gray value representing the background, c_{circle} is the offset of the circle with respect to the background, r_0 is the circle radius in pixels, x_0 and y_0 are the coordinates of the center of circle in pixels.

The sigmoid function

$$sigmoid(s,r,r_0) = 0.5 \cdot \left(1 - \frac{s\cdot(r-r_0)}{1+|s\cdot(r-r_0)|}\right) \qquad (3)$$

represents the circle with an adaptive mean edge sharpness controlled by the parameter s. As the sharpness parameter s increases, the edge gets sharper. This sigmoid function is chosen for reasons of faster calculations, other sigmoid functions may give similar results.

The used cost function F is the residual sum of squares over the regions of interest R

$$F = \sum_{i,(x_i,y_i)\in R}\left(I(x_i,y_i) - I_{circle}(x_i,y_i)\right)^2 \qquad (4)$$

For minimizing the cost function a gradient based optimization method (ADAM) is used.

In Fig. 8 example images of the measured image data $I(x_i,y_i)$, the model function $I_{circle}(x_i,y_i)$ and the corresponding image of residuals $I(x_i,y_i) - I_{circle}(x_i,y_i)$ are shown.

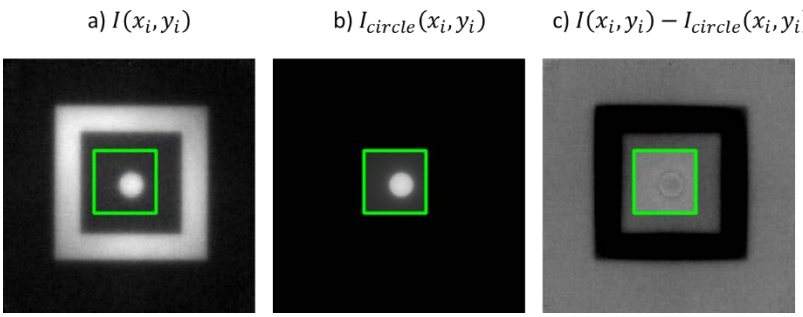

Figure 8. CS reconstruction image $I(x_i,y_i)$ (a), model function $I_{circle}(x_i,y_i)$ (b), and image of residuals $I(x_i,y_i) - I_{circle}(x_i,y_i)$ (c). The data fit is only applied on the region of interest depicted by the green box. A mean gray value of 127 represents zero in the image of residuals.

For different integration times, 50 frames are captured or reconstructed from CS measurements respectively. Each frame is fitted by the model function $I_{circle}(x_i,y_i)$ and the resulting fit parameters $(x_0, y_0, s, c_{background}, c_{circle}, r_0)$ and mean and standard deviation calculated over the 50 frames. The center of circle fluctuations are then calculated as

$$\sigma_{center} = \sqrt{\sigma_{x_0}^2 + \sigma_{y_0}^2} \qquad (5)$$

where $\sigma_{x_0}^2$ and $\sigma_{y_0}^2$ are the standard deviations of the horizontal and vertical center positions x_0 and y_0.

3.4 Data evaluation

The comparison of the two imaging system concepts is based on the analysis of the position fluctuations of the test target. For the FPA-based camera, the position fluctuations induced by air turbulence are expected to be dependent on the sensor integration time. A longer exposure time compensates the position fluctuations caused by the turbulence at the expense of image sharpness. The assumption is supported by the data shown in Fig. 9, where the fluctuations (standard deviation values) of the center of circle are displayed. Under normal atmospheric conditions (black squares), the standard deviation of the circle position remains almost constant for integration times between 0.2 and 50 ms. A slightly increased value was calculated for 0.1 ms that might be explained by the low signal-to-noise ratio. The intense changing of the circle centroids in severe turbulence conditions (blue squares) are about ten times higher than for normal atmospheric conditions. Increasing the

exposure time over 20 ms, the position fluctuations are starting to get weaker, a behaviour well-known for short and long exposure time imagery in turbulence conditions.

For comparison, CS measurements have been performed under similar conditions. Several series of images have been recorded under normal and strong turbulent atmosphere. The reconstruction of one image was based on 16000 modulation patterns (~ 25% compression ratio) selected according to methods B, C and D of Section 2.2.

However, a direct comparison of the two systems is not trivial since the CS procedure may not be characterized by a parameter equivalent to the FPA exposure time. A measurement based on 16000 modulation patterns takes about 4 s, but this mainly because of mirror frequency. The acquisition of a pattern is performed in either 5 µs or 50 µs. So the time included in one image reconstruction is the number of patterns multiplied by the acquisition time, resulting in 80 ms and 800 ms. This range is marked green in Fig. 9. The range of position fluctuation estimated for the CS data is plotted in yellow for strong turbulence and grey for no turbulence conditions. As shown the overlap of time and ranges compares well with the integration time dependency found for the camera system. It can be concluded that the turbulence has similar influence on CS and FPA based systems.

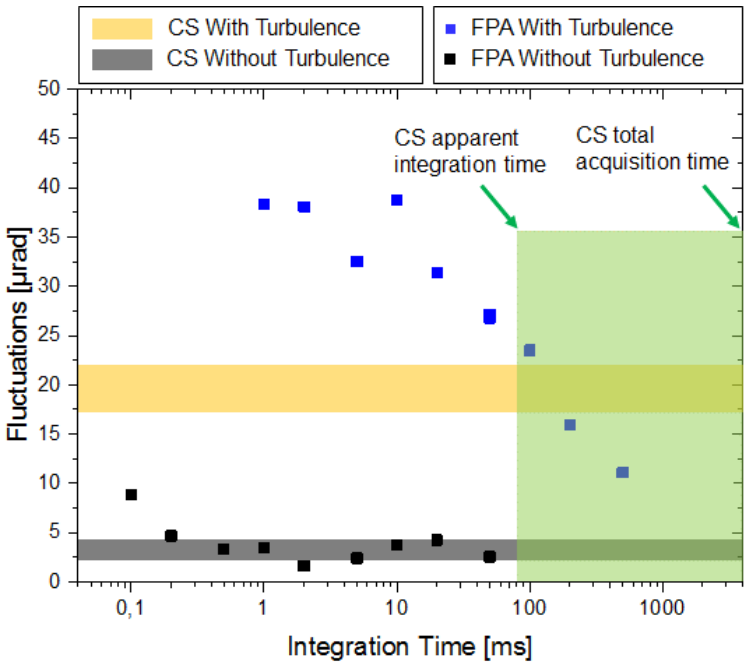

Figure 9: Standard deviation of the centre of circle under normal and strong turbulence conditions.

4.0 SUMMARY

Compressive sensing measurements have been performed using coherent and non-coherent illumination sources in SWIR and visible spectral range. The encoding patterns based on Hadamard matrix have been selected via four different methods. The results comparison shows the scene adapted pattern selection outperforming the other tested methods. However, its requirement for a full-resolution acquisition implies long data capturing time and increased data volume. Therefore the method based on image collection pattern evaluation may be advantageous in many applications.

Turbulence influence on a SWIR CS imaging was investigated in comparison to an InGaAs-FPA based camera. To do so strong turbulence was created in laboratory by a heating source. Series of images of a test target have been captured or reconstructed from CS measurements respectively, under these conditions and without turbulence. The analysis of the position fluctuations of the target allowed quantifying the influence of the turbulence. The measurements showed that the CS reconstructed images experience similar turbulence-induced effects like the FPA-based camera. The experimental study could not demonstrate an advantage for one of the two image acquisition concepts.

The investigated CS configuration was based on the modulation of the target back-reflected light. Future work will include the analysis of active CS systems based on both modulated illumination light as well as ~~on~~ modulated back-reflected light.

ACKNOWLEDGEMENTS

The authors are grateful to Richard Frank, Frank Willutzki and Frank van Putten for technical assistance.

REFERENCES

[1] Du Bosq, T. et al, "An overview of joint activities on computational imaging and compressive sensing systems by NATO SET-232," Proc. SPIE 10669, 10669OH (2018).

[2] Duarte, M.F., Davenport, M.A., Takhar, D., Laska, J.N., Sun, T., Kelly, K.F., Baraniuk, R.G., "Single-pixel imaging via compressive sampling," IEEE Signal Proc. Mag., 25 (2008), pp. 83-91.

[3] Paunescu, G., Lutzmann, P., Wegner, D., "Compressive sensing for active imaging in SWIR spectral range," Proc. SPIE 10796, 107960A (2018).

[4] Baraniuk, R. et al., "Dual-port measurements of light reflected from micromirror array," Patent No. US008717466B2 (2014).

[5] Yu, W-K., Liu, X-F., Yao, X-R., Wang, C., Zhai, Y. and Zhai, G-J., "Complementary compressive imaging for the telescopic system," Scientific Reports 4, Article Number 5834 (2014).

[6] Yu, W.K., Yao, X.R., Liu, X.F., Li, L.Z., and Zhai, G.J., "Three-dimensional single-pixel compressive reflectivity imaging based on complementary modulation," Appl. Opt. 54, 363-367 (2015).

[7] Soldevila, F., Clemente, P., Tajahuerce, E., Uribe-Patarroyo, N., Andrés, P., and Lancis, J., "Computational imaging with a balanced detector," Sci. Rep. 6(1), 29181 (2016).

[8] Radwell, N., Mitchell, K. J., Gibson, G., Edgar, M., Bowman, R., and Padgett, M. J., "Single-pixel infrared and visible microscope," Optica 1(5), 285–289 (2014).

[9] Sun, M.-J., Meng, L.-T., Edgar, M.P., Padgett, M.J., and Radwell, N., "A Russian Dolls ordering of the Hadamard basis for compressive single-pixel imaging," Scientific Reports 7, Article Number 3464 (2017).

[10] Kanjilal, P.P., Adaptive prediction and predictive control, Peter Peregrinus Ltd. (on behalf of I.E.E. London), 1995.

[11] Fletcher, R. and Reeves, C. M., "Function minimization by conjugate gradients", Comput. J. 7, 149–154 (1964).

[12] Kiefer, J., "Sequential minimax search for a maximum", Proceedings of the American Mathematical Society 4 (3), 502–506 (1953).

[13] Wang, Z., Bovik, A. C., Sheikh, H. R., and Simoncelli, E. P., "Image Quality Assessment: From Error Visibility to Structural Similarity", IEEE Transactions on Image Processing 13(4), 600–612 (2004).